

# Mid-infrared gas filled photonic crystal fiber laser based on population inversion

Andrew M. Jones,<sup>1</sup> A. V. Vasudevan Nampootheri,<sup>2</sup> Amarin Ratanavis,<sup>2</sup> Tobias Fiedler,<sup>2</sup>  
Natalie V. Wheeler,<sup>3</sup> François Couny,<sup>3</sup> Rajesh Kadel,<sup>1</sup> Fetah Benabid,<sup>3</sup>  
Brian R. Washburn,<sup>1</sup> Kristan L. Corwin<sup>1\*</sup> and Wolfgang Rudolph<sup>2</sup>

<sup>1</sup>Department of Physics, Kansas State University, Manhattan, KS 66506, USA

<sup>2</sup>Department of Physics, University of New Mexico, Albuquerque, NM 87131, USA

<sup>3</sup>Centre for Photonics and Photonic Materials, Department of Physics, University of Bath, BA2, 7AY, UK

\*corwin@phys.ksu.edu

**Abstract:** We demonstrate for the first time an optically pumped gas laser based on population inversion using a hollow core photonic crystal fiber (HC-PCF). The HC-PCF filled with  $^{12}\text{C}_2\text{H}_2$  gas is pumped with  $\sim 5$  ns pulses at  $1.52 \mu\text{m}$  and lases at  $3.12 \mu\text{m}$  and  $3.16 \mu\text{m}$  in the mid-infrared spectral region. The maximum measured laser pulse energy of  $\sim 6$  nJ was obtained at a gas pressure of 7 torr with a fiber with 20 dB/m loss near the lasing wavelengths. While the measured slope efficiencies of this prototype did not exceed a few percent due mainly to linear losses of the fiber at the laser wavelengths, 25% slope efficiency and pulse energies of a few mJ are the predicted limits of this laser. Simulations of the laser's behavior agree qualitatively with experimental observations.

©2011 Optical Society of America

**OCIS codes:** (140.4130) Molecular gas lasers; (140.3070) Infrared and far-infrared lasers; (060.5295) Photonic crystal fibers.

---

## References and links

1. R. Colombelli, K. Srinivasan, M. Troccoli, O. Painter, C. F. Gmachl, D. M. Tennant, A. M. Sergent, D. L. Sivco, A. Y. Cho, and F. Capasso, "Quantum cascade surface-emitting photonic crystal laser," *Science* **302**(5649), 1374–1377 (2003).
2. J. Faist, F. Capasso, D. L. Sivco, C. Sirtori, A. L. Hutchinson, and A. Y. Cho, "Quantum cascade laser," *Science* **264**(5158), 553–556 (1994).
3. R. F. Curl, F. Capasso, C. Gmachl, A. A. Kosterev, B. McManus, R. Lewicki, M. Pusharsky, G. Wysocki, and F. K. Tittel, "Quantum cascade lasers in chemical physics," *Chem. Phys. Lett.* **487**(1-3), 1–18 (2010).
4. J. E. McCord, H. C. Miller, G. Hager, A. I. Lampson, and P. G. Crowell, "Experimental investigation of an optically pumped mid-infrared carbon monoxide laser," *IEEE J. Quantum Electron.* **35**(11), 1602–1612 (1999).
5. J. E. McCord, A. A. Ionin, S. P. Phipp, P. G. Crowell, A. I. Lampson, J. K. McIver, A. J. W. Brown, and G. D. Hager, "Frequency-tunable optically pumped carbon monoxide laser," *IEEE J. Quantum Electron.* **36**(9), 1041–1052 (2000).
6. H. C. Miller, D. T. Radzykewycz, and G. Hager, "An optically pumped midinfrared HBr laser," *IEEE J. Quantum Electron.* **30**(10), 2395–2400 (1994).
7. A. V. V. Nampootheri, A. Ratanavis, N. Campbell, and W. Rudolph, "Molecular  $\text{C}_2\text{H}_2$  and HCN lasers pumped by an optical parametric oscillator in the  $1.5\text{-}\mu\text{m}$  band," *Opt. Express* **18**(3), 1946–1951 (2010), <http://www.opticsinfobase.org/oe/abstract.cfm?URI=oe-18-3-1946>.
8. T. Y. Chang, and T. J. Bridges, "Laser action at 452, 496, and 541  $\mu\text{m}$  in optically pumped  $\text{CH}_3\text{F}$ ," *Opt. Commun.* **1**(9), 423–426 (1970).
9. T. Y. Chang, and O. R. Wood, "An optically pumped  $\text{CO}_2$  laser," *IEEE J. Quantum Electron.* **8**(6), 598 (1972).
10. H. R. Schlossberg, and H. R. Fetterman, "Optically pumped vibrational transition laser in OCS," *Appl. Phys. Lett.* **26**(6), 316–318 (1975).
11. T. Ehrenreich, B. Zhdanov, T. Takekoshi, S. P. Phipps, and R. J. Knize, "Diode pumped cesium laser," *Electron. Lett.* **41**(7), 415–416 (2005).
12. C. S. Kletecka, N. Campbell, C. R. Jones, J. W. Nicholson, and W. Rudolph, "Cascade lasing of molecular HBr in the four micron region pumped by a Nd:YAG laser," *IEEE J. Quantum Electron.* **40**(10), 1471–1477 (2004).
13. F. Benabid, J. C. Knight, G. Antonopoulos, and P. S. J. Russell, "Stimulated Raman scattering in hydrogen-filled hollow-core photonic crystal fiber," *Science* **298**(5592), 399–402 (2002).
14. A. R. Bhagwat, and A. L. Gaeta, "Nonlinear optics in hollow-core photonic bandgap fibers," *Opt. Express* **16**(7), 5035–5047 (2008), <http://www.opticsinfobase.org/oe/abstract.cfm?URI=oe-16-7-5035>.

15. F. Benabid, G. Bouwmans, J. C. Knight, P. S. Russell, and F. Couny, "Ultra-high efficiency laser wavelength conversion in a gas-filled hollow core photonic crystal fiber by pure stimulated rotational Raman scattering in molecular hydrogen," *Phys. Rev. Lett.* **93**(12), 123903 (2004).
16. F. Couny, F. Benabid, P. J. Roberts, P. S. Light, and M. G. Raymer, "Generation and photonic guidance of multi-octave optical-frequency combs," *Science* **318**(5853), 1118–1121 (2007).
17. R. F. Cregan, B. J. Mangan, J. C. Knight, T. A. Birks, P. S. Russell, P. J. Roberts, and D. C. Allan, "Single-mode photonic band gap guidance of light in air," *Science* **285**(5433), 1537–1539 (1999).
18. J. D. Shephard, W. N. Macpherson, R. R. J. Maier, J. D. C. Jones, D. P. Hand, M. Mohebbi, A. K. George, P. J. Roberts, and J. C. Knight, "Single-mode mid-IR guidance in a hollow-core photonic crystal fiber," *Opt. Express* **13**(18), 7139–7144 (2005), <http://www.opticsinfobase.org/oe/abstract.cfm?URI=oe-13-18-7139>.
19. P. S. Light, F. Couny, Y. Y. Wang, N. V. Wheeler, P. J. Roberts, and F. Benabid, "Double photonic bandgap hollow-core photonic crystal fiber," *Opt. Express* **17**(18), 16238–16243 (2009), <http://www.opticsinfobase.org/oe/abstract.cfm?URI=oe-17-18-16238>.
20. J. v. Neumann, and E. Wigner, "Über merkwürdige diskrete Eigenwerte," *Phys. Z.* **30**, 465 (1929).
21. F. Benabid, F. Couny, J. C. Knight, T. A. Birks, and P. S. Russell, "Compact, stable and efficient all-fibre gas cells using hollow-core photonic crystal fibres," *Nature* **434**(7032), 488–491 (2005).
22. J. D. Shephard, J. D. C. Jones, D. P. Hand, G. Bouwmans, J. C. Knight, P. S. Russell, and B. J. Mangan, "High energy nanosecond laser pulses delivered single-mode through hollow-core PBG fibers," *Opt. Express* **12**(4), 717–723 (2004), <http://www.opticsinfobase.org/oe/abstract.cfm?URI=oe-12-4-717>.
23. M. C. Heaven, J. Han, and K. Freel, "Rotational and vibrational energy transfer from the first overtone stretch of acetylene," presented at the Sixty-fifth International Symposium on Molecular Spectroscopy, Columbus, Ohio, 21–25 June 2010.
24. HITRAN database, <http://www.cfa.harvard.edu/HITRAN/>.
25. W. C. Swann, and S. L. Gilbert, "Pressure-induced shift and broadening of 1510-1540-nm acetylene wavelength calibration lines," *J. Opt. Soc. Am. B* **17**(7), 1263–1270 (2000).
26. J. W. Dawson, M. J. Messerly, R. J. Beach, M. Y. Shverdin, E. A. Stappaerts, A. K. Sridharan, P. H. Pax, J. E. Heebner, C. W. Siders, and C. P. J. Barty, "Analysis of the scalability of diffraction-limited fiber lasers and amplifiers to high average power," *Opt. Express* **16**(17), 13240–13266 (2008), <http://www.opticsinfobase.org/oe/abstract.cfm?URI=oe-16-17-13240>.
27. A. Ratanavis, N. Campbell, and W. Rudolph, "Feasibility study of optically pumped molecular lasers with small quantum defect," *Opt. Commun.* **283**(6), 1075–1080 (2010).

## 1. Introduction

The need for portable, tunable lasers in the mid-infrared (mid-IR) is compelling. This eye-safe spectral region offers high atmospheric transmission essential to applications such as remote sensing and space-based terrestrial imaging and communications. Quantum cascade lasers (QCLs) have emerged as promising mid-IR sources and have even been integrated with photonic crystal resonator structures [1]. However, QCLs typically operate from 4 to 10  $\mu\text{m}$  [2], become multi-mode at high powers, and have thermal management challenges [3]. Optically pumped gas lasers, in which a narrow-band pump laser is resonant with the gas-phase medium, can be pumped in the near-infrared to produce mid-IR emissions [4–7], but remain bulky and cumbersome. In this paper we report on the demonstration of a new class of optically pumped gas laser based on population inversion. The gas is confined to a HC-PCF whose transmission spans several octaves to reach the mid-IR spectral region. The laser produces light near 3  $\mu\text{m}$  when pumped at  $\sim 1.5 \mu\text{m}$ , offering a potentially robust, efficient, and compact means of producing step-tunable eye-safe mid-IR radiation well suited to a multitude of applications.

Compared to solid state laser media, gases have attractive properties including high damage thresholds, the possibility of heat dissipation through gas circulation, relatively large gain cross-sections, and emission frequencies from the near to far-infrared. A variety of optically pumped gas lasers have been demonstrated, from the earliest  $\text{CH}_3\text{F}$  [8],  $\text{CO}_2$  [9], and  $\text{OCS}$  [10], to alkali vapor [11],  $\text{CO}$  [4, 5],  $\text{HBr}$  [6],  $\text{C}_2\text{H}_2$  and  $\text{HCN}$  [7]. Some of these mid-IR lasers can be pumped via ro-vibrational overtones at wavelengths in the telecommunication bands where commercial pump sources are well established and readily available. Early work with  $\text{HBr}$  gas cells pumped at 1.3  $\mu\text{m}$  has demonstrated lasing at  $\sim 4 \mu\text{m}$  with conversion efficiencies of  $\sim 25\%$  [6]. More recently cascade lasing in  $\text{HBr}$  at wavelengths near 4  $\mu\text{m}$  suggests that conversion efficiencies exceeding 50% are possible [12]. The main disadvantage that has limited widespread use of gas lasers and prevented their integration into many practical optical systems is the bulky, fragile packaging necessary to achieve long optical path lengths and extract appreciable laser output due to the dilute nature of gas media.

The problem of weak interaction between light and gas has been solved with the advent of gas-filled HC-PCF, whereby light and the gas phase are confined to areas on the order of  $100 \mu\text{m}^2$  over distances of tens of meters [13]. A variety of nonlinear optical phenomena [14] have been demonstrated using HC-PCF including the development of a gas-filled fiber Raman laser [15] and a multi-octave spanning Raman frequency comb [16]. HC-PCF [17] consists of a hollow, air-filled core surrounded by a periodic array of smaller holes. Two classes of HC-PCF have emerged. The first guides via a photonic bandgap [17] and has demonstrated narrow-band guidance near  $3 \mu\text{m}$  [18], but not the octave-spanning guidance [19] required for this work. The second, represented by kagome HC-PCF [13], guides via a mechanism akin to Von Neumann and Wigner states [20] whereby core and cladding modes can coexist essentially without coupling to each other. As a result of this salient feature, kagome HC-PCF permits ultra-broad, multi-octave spanning spectral guidance [13], with reasonably low loss ( $< 1 \text{ dB/m}$ ) across a broad spectrum. These fibers can be spliced to solid-core fibers, creating compact, robust sealed gas cells that can readily be integrated into devices [21].

## 2. Experimental gas-filled fiber laser setup

### 2.1 Fiber specifics

The kagome fiber used here is the first to demonstrate multi-octave spanning guidance that includes the mid-IR; its cross section and guided modes are shown in Fig. 1a-c. The fiber is formed from high purity, low OH content ( $\sim 0.1 \text{ ppm}$ ) fused silica using a stack and draw technique. Light out to  $\sim 3.4 \mu\text{m}$  is reasonably well guided in the fiber, even though fused silica exhibits strong absorption at wavelengths beyond  $\sim 3 \mu\text{m}$ , because the light that propagates is mostly confined to the hollow central core. A 3-ring cladding surrounds a single-cell defect core  $\sim 45 \mu\text{m}$  in diameter, with excellent guidance at the pump wavelength of  $1.52 \mu\text{m}$  and weak guidance near the laser wavelengths in the mid-IR. Figure 1d shows the measured and calculated fiber loss spectrum and the calculated group velocity. Standard cut-back measurements were performed to measure the wavelength dependent loss of the fiber. A broadband optical source and an optical spectrum analyzer were used at wavelengths below  $1.75 \mu\text{m}$ . The data at  $3.16 \mu\text{m}$  was taken using the output of an optical parametric oscillator (OPO) coupled through the fiber and detected by a PbSe photodetector. The measured fiber loss is less than  $0.5 \text{ dB/m}$  near  $1.5 \mu\text{m}$  and is  $20 \text{ dB/m}$  at  $3.16 \mu\text{m}$ . More data points in the region beyond  $1.75 \mu\text{m}$  can be taken but require a more stable OPO output mode and pulse

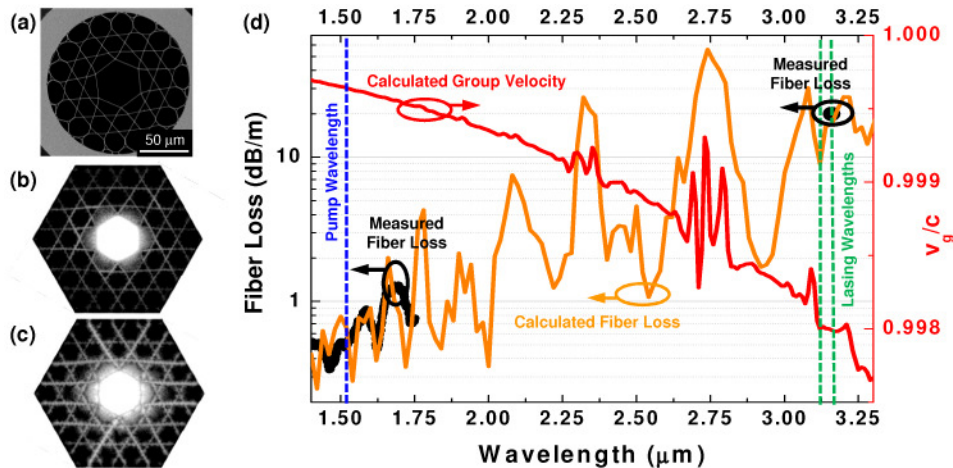


Fig. 1. Kagome HC-PCF fiber structure, guided mode profiles, and loss spectrum and group velocity. (a) Scanning electron microscope image of the cross section of the fiber used in the experiment. The diameter of the hollow core varies from  $42.4 - 48.3 \mu\text{m}$ . The fiber pitch is  $\sim 23 \mu\text{m}$ , and the typical strut thickness is  $\sim 0.4 \mu\text{m}$ . Calculated core mode profiles at (b)  $1.52 \mu\text{m}$  and (c)  $3.12 \mu\text{m}$ . (d) Measured (black circles) and calculated (orange) fiber loss with the calculated group velocity (red).

energy while tuning the wavelength than was available. The calculated fiber loss is a result of the confinement loss of the fiber, which arises partially from the fact that the microstructured cladding region is finite in size, and partly from the intrinsic guidance mechanism of the fiber whereby there is a residual coupling between the cladding continuum modes and the guided core modes [16]. This results in a light leakage from core guided modes through the microstructured cladding into the outer bulk silica. In our work the confinement loss was calculated using finite element analysis software from JCMwave which was also used to solve the fiber modes. The measured and calculated fiber losses are in good agreement, allowing fast and accurate numerical customization and optimization of fiber loss profiles in the future.

## 2.2 Laser configuration

The laser setup is shown in Fig. 2a. The heart of the laser is the hollow PCF waveguide, which contains the gas-phase gain medium and serves as the laser cavity by guiding only emissions that fall within the guided modes of the fiber, effectively providing spectral and spatial feedback leading to coherent laser oscillation. Both ends of the kagome fiber are supported inside vacuum chambers within 1 cm of the windows, as shown in Fig. 2b, allowing light to be coupled through the evacuated fiber. Experiments were performed with 1.65-m and 0.95-m long HC-PCFs. Filling the evacuated fiber with acetylene ( $^{12}\text{C}_2\text{H}_2$ ) gas to equilibrium pressures of up to tens of torr takes only minutes owing to the relatively large fiber core, and implies average flow rates of  $\sim 10^{10}$  molecules/s. Use of a 19-cell defect fiber with core diameters of 50-70  $\mu\text{m}$  would further decrease the filling times and allow even faster flow rates. BK7 glass optics couple in pump light at  $\sim 1.5 \mu\text{m}$ , while  $\text{CaF}_2$  optics couple laser light out. The laser is pumped with an OPO producing pulses roughly 5 ns in duration with a bandwidth of about 3.5 GHz tuned to resonance with the  $\nu_1 + \nu_3$  (R7) ro-vibrational transition in  $^{12}\text{C}_2\text{H}_2$ ,  $\lambda = 1521.06 \text{ nm}$ . The pump pulse energy incident on the fiber is kept below 100  $\mu\text{J}$  to avoid damage [22]. Polished germanium wafers filter transmitted pump light from mid-IR laser pulses exiting the fiber. The measured output mode profile is shown in Fig. 2c. A fast InGaAs photodetector measures pump pulse energy while a fast HgCdTe photodetector observes mid-IR pulses.

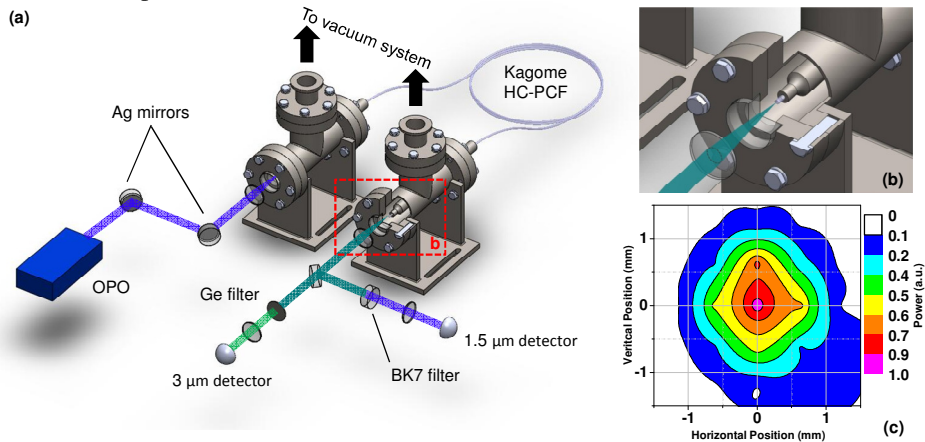


Fig. 2. Experimental setup and laser beam profile. (a) Pulses from an OPO with a center wavelength of  $\sim 1.5 \mu\text{m}$  and 5 ns duration (shown in blue) are coupled into a kagome structured HC-PCF containing low pressure acetylene gas. Pump radiation is absorbed by the gas and laser radiation is detected from ro-vibrational transitions at wavelengths in the mid-IR (shown in green). Laser energy is filtered from pump energy by a polished germanium wafer and detected by a fast, room-temperature HgCdTe photovoltaic detector. (b) Close-up showing a fiber end suspended in a vacuum chamber. (c) Far-field mode profile: power of the collimated 3  $\mu\text{m}$  beam passing through a 750- $\mu\text{m}$  diameter circular aperture as the aperture is scanned transverse to the beam.

### 3. Experimental results and discussion

Pump pulses excite acetylene molecules from the  $J = 7$  rotational state of the vibrational ground state to the  $J = 8$  rotational state of the  $\nu_1 + \nu_3$  vibrational manifold (Fig. 3 inset). Acetylene molecules can then leave this excited state via radiative transitions to the  $\nu_1$  vibrational state with corresponding emission wavelengths in the  $3 \mu\text{m}$  region. Alternatively, molecules initially in the excited state may exchange energy nonradiatively through intermolecular collisions and collisions with the fiber wall, processes that can decrease the overall laser efficiency. The relative contribution of wall collisions is expected to be small at pressures above 2 torr, where the calculated mean free path of gas molecules is  $< 20 \mu\text{m}$ . Just as in the free space acetylene laser [7], two peaks in the laser spectrum are seen at  $3.12 \mu\text{m}$  and  $3.16 \mu\text{m}$  (Fig. 3). These peaks correspond to the dipole allowed transitions ( $\Delta J = \pm 1$ ) from the  $J = 8, \nu_1 + \nu_3$  excited state to the  $J = 7$  and  $J = 9$  rotational states of the  $\nu_1$  vibrational state. The absence of any other peaks indicates insufficient time for molecules in the excited state to rotationally mix through intermolecular collisions before the onset of lasing and vibrational relaxation. Measured total removal rates from the upper pump level are  $\sim 10^{-9} \text{ cm}^3 \text{ s}^{-1}$  [23].

Figure 4 shows laser pulse energies measured at various acetylene gas pressures for a fixed pump energy. The maximum laser pulse energy is  $\sim 6 \text{ nJ}$  measured at an acetylene pressure of 7 torr. Delays between the transmitted pump and laser pulses do not exceed 5 ns. Laser pulse durations were observed to be between  $\sim 3 \text{ ns}$  and  $5 \text{ ns}$ . The lasing threshold occurs at about 200 nJ of coupled pump pulse energy and varies with pressure. The slope efficiency is only  $\sim 1\%$  in comparison with about 10% from the free space acetylene laser [7], but can be improved by reducing the fiber attenuation at the laser wavelength through optimization of the fiber length and pitch. Neglecting relaxation processes, the maximum possible slope efficiency for this laser is 25% and is a result of saturating both the pump and lasing transitions. In the limit of lossless fiber and 25% efficiency the ultimate achievable pulse energies to expect from these lasers should be limited by the fiber damage threshold. Damage fluences for 8-ns pulses at 1064 nm on the order of  $100 \text{ J/cm}^2$  were observed for the cladding in HC-PCFs [22], which roughly corresponds to the critical fluence of bulk fused silica. In contrast, a roughly 10 times higher fluence was demonstrated by the guided mode without causing catastrophic damage [22]. If we assume that the damage fluence scales as the square root of the pulse duration and is rather wavelength independent we obtain an estimate for the maximum pump energy that can be coupled into our fiber on the order of 10 mJ, resulting in a maximum laser energy of a few mJ. This energy limit can be increased through the use of larger core fibers, longer pulse durations and more efficient lasing schemes.

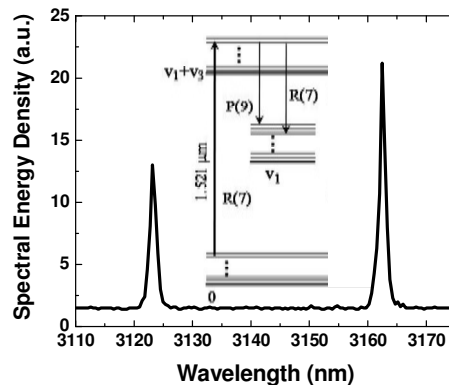


Fig. 3. Spectrum of the acetylene-filled PCF laser. The laser spectrum was taken using a grating spectrometer with  $\sim 1 \text{ nm}$  resolution. The two peaks correspond to transitions from the  $J = 8, \nu_1 + \nu_3$  pump state to the  $J = 7$  and  $J = 9, \nu_1$  state, corresponding to wavelengths of  $3123.2 \text{ nm}$  and  $3162.4 \text{ nm}$ , respectively. The inset shows pertinent transitions on an energy level diagram.

#### 4. Modeling results

We use a simple model to qualitatively predict the trends observed in the experiment. The model system is comprised of only three states: a ground state, the pumped excited state, and a terminal excited state with no direct path for population to transfer to or from the ground state during our time scale of interest. The absorption cross-section for the pump transition is estimated as  $7.7 \times 10^{-18} \text{ cm}^2$  [24]. Since data for the stimulated emission cross-section for the lasing transition is not available, we assume that it is of the same order of magnitude as that for the  $\nu_3 \rightarrow \nu_0$  transition, which is estimated to be  $\sim 2.2 \times 10^{-16} \text{ cm}^2$  using the known Einstein A coefficient [24]. A Gaussian pump pulse 5 ns long and 2 GHz in bandwidth spectrally centered on resonance with the gas at  $1.52 \text{ }\mu\text{m}$  enters the fiber, creating a population inversion. The laser pulse develops from spontaneous emission and co-propagates with the pump; linear fiber losses are accounted for. The model predicts an optimum pressure, experimentally observed in Fig. 4, which is a function of the fiber length and pump energy. The optimum pressure essentially occurs when a given pump pulse energy just creates enough gain to balance the fiber loss at the end of the fiber. Any further increase in pressure causes additional pump absorption, resulting in more loss than gain before the fiber end. A smaller pressure dependent effect arises from the linewidth of the pump transition ( $\sim 1 \text{ GHz}$  at 7 torr [25]).

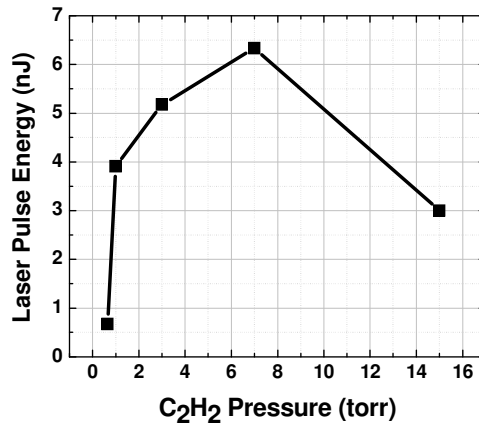


Fig. 4. Measured dependence of laser pulse energy on gas pressure. Laser pulse energy increases with  $^{12}\text{C}_2\text{H}_2$  gas pressure and peaks at  $\sim 6 \text{ nJ}$  at 7 torr. The pump pulse energy launched into the 1.65 m long fiber was about  $1 \text{ }\mu\text{J}$ .

The measured and predicted laser pulse energies as a function of pump pulse energy are shown in Fig. 5a and Fig. 5b respectively. The experimental and calculated data are in good qualitative agreement, showing exponential-like small signal gain followed by the onset of saturation as the pump pulse begins to saturate the gas absorption at the end of the fiber. Only relative comparisons between experiment and calculation can be made because the exact fiber-to-free space coupling efficiencies are not known. Cut-back measurements to determine the actual efficiencies are complicated by time-dependent fluctuations in the spatial mode and center frequency of pump pulses from the OPO. Mid-IR laser output as a function of fiber length as predicted by the model is shown in Fig. 5c. When pumping at  $6 \text{ }\mu\text{J}$  (solid curves), the first knee present in the laser energy curve occurs when the saturated gain approximately equals the linear fiber loss for the laser radiation. The plateau in the output power persists while the pump is able to maintain (saturated) gain that equals the linear fiber loss for the laser radiation, ending when the depleted pump cannot maintain sufficient population inversion. Figure 5d-f show the evolution of pump (blue) and laser (green) pulse power calculated at different positions along the length of the fiber for a launched pump (gray) pulse energy of  $6 \text{ }\mu\text{J}$ . Initially the laser pulse develops at the leading edge of the undepleted pump pulse (Fig. 5d). As the leading edge of the pump is absorbed and saturates the transition, the

positive net gain window shifts towards later times during the pump pulse. As a result the laser pulse broadens and its center moves backwards (Fig. 5e). At long fiber lengths the pump is almost completely absorbed and the laser pulse energy begins to decrease as the pump can no longer sustain the inversion necessary to compensate the fiber loss (Fig. 5f). Additionally, the temporal width of the laser pulse broadens as it propagates along the fiber and never exceeds the 5-ns duration of the launched pump pulse.

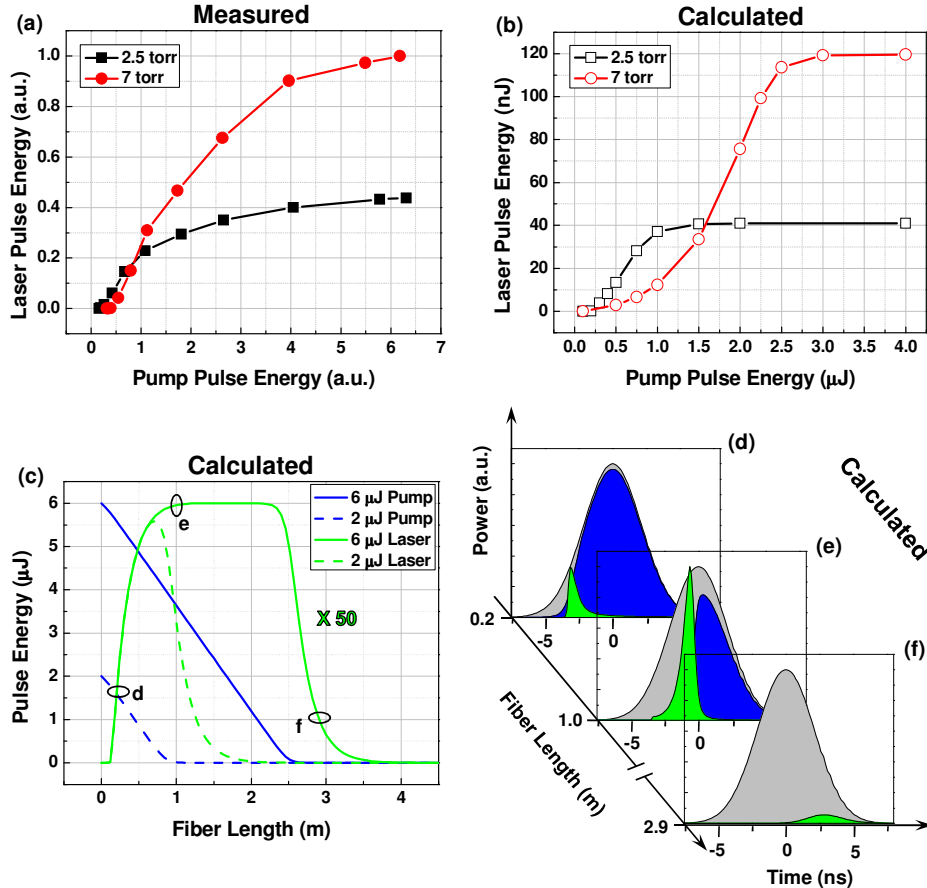


Fig. 5. Experimental and calculated laser pulse energy dependence on pump energy and fiber length. Laser pulse energy (a) measured and (b) calculated for various levels of pump pulse energy coupled into a 0.9 m long fiber containing  $^{12}\text{C}_2\text{H}_2$  at pressures of 2.5 and 7 torr. (c) The calculated laser (green curves) and pump (blue curves) pulse energies at different positions along the fiber length containing 7 torr of  $^{12}\text{C}_2\text{H}_2$  gas for two different launched pump pulse energies; the laser energy is multiplied by a factor of 50. (d-f) The calculated temporal profiles of the laser (green), and transmitted pump (blue) pulses along with the launched pump (gray) pulse at several positions along the fiber, where the laser power is scaled up by a factor of 5.5.

## 5. Conclusions

Realization of the first gas fiber laser based on population inversion holds great promise for coherence generation applications as well as for engineering high power, portable and robust, all fiber mid-IR sources in the future. One can effectively engineer gas-filled fiber laser sources at numerous wavelengths difficult to obtain with other technologies by carefully selecting the gas and designing the optical fiber. The gas must absorb at wavelengths where inexpensive, high-power pump sources exist, and lase at a wavelength of interest; the fiber should be highly transmissive at both the pump and laser frequencies while suppressing lasing on unwanted transitions. While the performance of solid core fiber lasers at high powers can

be limited by the onset of nonlinear processes such as Brillouin and Raman scattering [26], gas-filled HC-PCF lasers can be expected to surpass these limits and have higher thresholds for damage, because no glass or other host material is present in the high intensity region of the propagating modes. Thus, phase-locking multiple gas-filled fiber lasers together may achieve higher ultimate powers than can be realized with solid-core systems. Sealing the fiber permits an all-fiber device, facilitating easy integration into optical systems. Continuous-wave (CW) operation of the laser is paramount for use in many potential applications. This will require fast repopulation of the ground state, which may favor asymmetric molecules or require buffer gases for tailored energy transfer. The addition of buffer gases may speed rotational mixing of the excited state population, remove population from unwanted vibrational states, and accelerate heat dissipation. Furthermore, extremely efficient molecular CW lasers with very small quantum defects [27] similar to alkali vapor lasers seem feasible with PCFs.

### **Acknowledgements**

This work was supported by the Air Force Office of Scientific Research (FA9550-08-1-0344), Army Research Office (W911NF-08-C-0106 and W911NF-08-1-0332), National Science Foundation (PHY-0722622), Joint Technology Office (W911NF-05-1-0507), Engineering and Physical Sciences Research Council (EP/E039162/1), and Precision Photonics Corp. We thank John Zavada for early discussions leading to the initial idea, P.J. Roberts for his assistance with the numerical modeling of the fiber, Neil Campbell for useful discussions, and Josh Perkins for preliminary work.